

# A self-calibration approach for optical long baseline interferometry imaging

Serge Meimon,<sup>1,\*</sup> Laurent M. Mugnier<sup>1</sup> and Guy Le Besnerais<sup>2</sup>

<sup>1</sup>*Office National d'Études et de Recherches Aéronautiques  
Département d'Optique Théorique et Appliquée  
BP 72, F-92322 Châtillon cedex, France*

<sup>2</sup>*Office National d'Études et de Recherches Aéronautiques  
Département Traitement de l'Information et Modélisation  
BP 72, F-92322 Châtillon cedex, France*

\*Corresponding author: [lastname@onera.fr](mailto:lastname@onera.fr)

Current optical interferometers are affected by unknown turbulent phases on each telescope. In the field of radio-interferometry, the self-calibration technique is a powerful tool to process interferometric data with missing phase information. This paper intends to revisit the application of self-calibration to Optical Long Baseline Interferometry (OLBI). We cast rigorously the OLBI data processing problem into the self-calibration framework and demonstrate the efficiency of the method on real astronomical OLBI dataset. © 2018 Optical Society of America

*OCIS codes:* Interferometry (120.3180); Image reconstruction-restoration (100.3020); Inverse problems (100.3190).

## 1. Introduction

Optical Long Baseline Interferometry (OLBI) aims to combine light collected by widely separated telescopes to access angular resolutions beyond the diffraction limit of each individual aperture. Long-baseline interferometers measure a discrete set of spatial frequencies of the observed object, or Fourier data. Due to instrumental complexity, current interferometers recombine only a few telescopes, and even several nights of observation lead to a very limited number of Fourier data; moreover, due to the atmospheric turbulence, it is very difficult to get reliable phase information from ground based interferometry [1]. Hence OLBI has to deal with severe under-determination and missing phase information.

The classical answer to under-determination is to use a parametric approach, *i.e.* to search for an object entirely described by a small set of parameters (for instance a circular object with a parametric attenuation profile). With a “good model”, such an approach allows a reliable and precise estimation of astrophysical parameters. A good model should limit as much as possible the number of free parameters, while allowing a description of all the object's features, because parametric inversion cannot reveal unguessed features. The  $\chi^2$  fit is often used as a model quality diagnosis,

since an inadequate model will often result in a poor fit to the data, thus revealing that a new model (with more parameters or different parameters) is needed. However, it does not reveal which new model must be adopted.

As progress in instrumental issues gives access to better frequency coverage, *i.e.* to potentially finer descriptions of the object, the choice of the model becomes more difficult. An alternate and complementary approach is then non-parametric reconstruction, which we will call "optical long baseline interferometric imaging" (OLBII). Imaging means that the object is described by a large set of parameters, such as coefficients of the object's decomposition in some spatial functional basis, while under-determination is tackled by regularization tools. Imaging is useful to understand the structure of a complex object when prior information is limited.

From the beginning, OLBII has been influenced by the remarkable techniques developed in radio-interferometry with very large baselines (VLBI) [2]. For instance, the "WIPE" OLBII technique of A. Lannes et al.[3] is inspired by the well-known CLEAN method [4]. As regards the missing phase problem, the self-calibration technique proposed in radio-interferometry by Cornwell and Wilkinson [5] underlies recent works in OLBII [6].

This paper intends to revisit the application of self-calibration to OLBI . Our contribution is three-fold:

1. we cast rigorously the OLBI data processing problem into the self-calibration framework, with consideration of the second-order statistics of the noise;
2. we propose WISARD (for Weak-phase Interferometric Sample Alternating Reconstruction Device), a self-calibration algorithm dedicated to OLBII, which uses the proposed data model within a Bayesian regularization approach;
3. we demonstrate the efficiency of WISARD on real astronomical OLBI dataset.

The paper is organized as follows: Section 2 describes the observation model of OLBI , briefly presents a Bayesian approach and discusses the main problems that are encountered because of the incomplete OLBI data. Section 3 is devoted to the derivation of a specific myopic model, which achieves a good approximation of the data model and leads to self-calibration techniques. One such technique, WISARD, is proposed in Section 4. Results of WISARD on simulated and real astronomical datasets are presented in Section 5. Our conclusions are given in Section 6. Most mathematical derivations are gathered in the Appendices.

## 2. Realistic observables in optical long baseline interferometry

### 2.A. Ideal interferometric data

Here we describe the ideal data, *i.e.* without aberrations, noise or turbulence effects, produced by a  $N_t$ -telescope interferometer observing a monochromatic source with wavelength  $\lambda$ . The brightness distribution of the source is denoted  $x(\boldsymbol{\xi})$ ,  $\boldsymbol{\xi}$  being angular coordinates on the sky. Individual telescopes  $T_k$  of the interferometer are located at three-space positions  $\vec{OT}_k$ , and we denote  $\mathbf{r}_k(t)$  the projection of  $\vec{OT}_k$  onto  $\mathcal{P}$ , the plane normal to the pointing direction. Because of the Earth's rotation, the pointing direction changes during an observing night, so these projected vectors are time dependent.

Each pair  $(T_k, T_l)$  of telescopes yields a fringe pattern with a 2D spatial frequency  $\boldsymbol{\nu}_{kl}(t) \triangleq \frac{\mathbf{u}_{kl}(t)}{\lambda}$ , where  $\mathbf{u}_{kl}(t)$  is the *baseline*

$$\mathbf{u}_{kl}(t) \triangleq \mathbf{r}_l(t) - \mathbf{r}_k(t), \quad (1)$$

*i.e.* the projection of the vector  $\overrightarrow{T_k T_l}$  onto  $\mathcal{P}$ .

Measuring the position and contrast of these fringes yields a phase  $\phi_{kl}^{\text{data}}(t)$  and an amplitude  $a_{kl}^{\text{data}}(t)$ , which can be grouped together in a complex visibility

$$y_{kl}^{\text{data}}(t) \triangleq a_{kl}^{\text{data}}(t) e^{i\phi_{kl}^{\text{data}}(t)}. \quad (2)$$

According to the Van Cittert-Zernike theorem [7], complex visibilities are *ideally* linked to the normalized Fourier Transform (FT) of  $x(\boldsymbol{\xi})$  at the 2D spatial frequency  $\boldsymbol{\nu}_{kl}(t)$  through

$$y_{kl}^{\text{data}}(t) = \eta_{kl}(t) \frac{\text{FT}[x(\boldsymbol{\xi})](\boldsymbol{\nu}_{kl}(t))}{\text{FT}[x(\boldsymbol{\xi})](\mathbf{0})}. \quad (3)$$

The *instrumental visibility*  $\eta_{kl}(t)$  accounts from the many potential sources of visibility loss: residual perturbations of the wavefront at each telescope, differential tilts between telescopes, differential polarization effects, non-zero spectral width, etc. In practice, the instrumental visibility is calibrated on a star reputed to be unresolved by the interferometer before the object of interest is observed, and is compensated for in the pre-processing of the raw data. Thanks to this calibration step, we replace  $\eta_{kl}(t)$  by 1 in equation (3).

For the sake of clarity, we consider a *complete*  $N_t$ -telescope array in what follows, *i.e.* one in which all the possible two-telescope baselines can be formed simultaneously, and a non-redundant interferometer configuration, where each baseline provides a different spatial frequency. Extension to incomplete and redundant settings is straightforward. Thus, at each time  $t$ , there are

$$N_b = \binom{N_t}{2} = \frac{N_t(N_t - 1)}{2} \quad (4)$$

complex observation equations such as (3).

Let us briefly introduce the discretized observation model. The sought brightness distribution  $x$  is represented by the coefficients  $\mathbf{x}$  of its projection onto some convenient spatial basis (box functions, sinc's, wavelets, prolate spheroidal functions, etc...). The normalized discrete-continuous Fourier matrix  $\mathbf{H}(t)$  maps the chosen discrete spatial representation into the real-valued instantaneous frequency coverage  $\{\boldsymbol{\nu}_{kl}(t)\}_{1 \leq k < l \leq N_t}$ , and we further define

$$\begin{cases} \mathbf{a}(\mathbf{x}, t) \triangleq |\mathbf{H}(t)\mathbf{x}| \\ \phi(\mathbf{x}, t) \triangleq \arg\{\mathbf{H}(t)\mathbf{x}\}. \end{cases} \quad (5)$$

## 2.B. Effect of atmospheric turbulence on short-exposure measurements

At optical wavelengths, atmospheric turbulence affects phase measurements through path length fluctuations. The statistics of these fluctuations can be described by a time scale parameter, the *coherence time*  $\tau_0$ , typically around 10 milliseconds, and by a space scale parameter, the *Fried*

parameter  $r_0$  [8]. We assume that the diameter of the elementary apertures is small relative to the Fried parameter, or that each telescope is corrected from the effects of turbulence by adaptive optics. The remaining turbulent effects on the interferometric measurements can be seen as a delay line between the two telescopes  $T_k$  and  $T_l$ , which affects short-exposure phase measurements through an additive *differential piston*  $\varphi_l(t) - \varphi_k(t)$ :

$$\phi_{kl}^{\text{data}}(t) = \phi_{kl}(\mathbf{x}, t) + \varphi_l(t) - \varphi_k(t) + \text{noise} [2\pi] \quad (6)$$

or, in a matrix formulation:

$$\phi^{\text{data}}(t) = \phi(\mathbf{x}, t) + \mathbf{B}\varphi(t) + \text{noise} [2\pi] \quad (7)$$

where  $N_b \times N_t$  operator  $\mathbf{B}$ , called the *baseline operator*, is defined in Appendix A.

Because the differential pistons are zero-mean, one might think that the object phase  $\phi(\mathbf{x}, t)$  could be recovered from (7) by averaging over many realizations of the atmosphere. However, for a long baseline relative to the Fried parameter, the optical path difference between apertures introduced by turbulence may be very much greater than the observation wavelength and thus lead to random pistons much larger than  $2\pi$ . The  $2\pi$ -wrapped perturbation that affects the phase (7) is then practically uniformly distributed in  $[0, 2\pi]$ . In consequence, averaging the short-exposure phases measurements (7) does not improve the signal-to-noise ratio.

In *phase referencing* techniques (see [9]), the turbulent pistons are measured in order to subtract them in (7). However powerful and promising, these methods require specific hardware and are not feasible for all sources. The only other way to obtain exploitable long-exposure data then is to form piston-free short-exposure observables *before* the averaging.

### 2.C. Piston-free short-exposure observables

Piston-free short-exposure phase observables are quantities  $f(\phi^{\text{data}}(t))$  in which the turbulent term  $\mathbf{B}\varphi(t)$  cancels out:

$$f(\phi^{\text{data}}(t)) = f(\phi(\mathbf{x}, t) + \mathbf{B}\varphi(t)) = f(\phi(\mathbf{x}, t)). \quad (8)$$

For an interferometric array of 3 telescopes or more, the *closure phases* [10] are one famous example, in which  $f$  is a linear operator performing triple-wise summation of the phases. For any set of three telescopes  $(T_k, T_l, T_m)$  the short-exposure visibility phase data are

$$\begin{cases} \phi_{kl}^{\text{data}}(t) = \phi_{kl}(\mathbf{x}, t) + \varphi_l(t) - \varphi_k(t) + \text{noise} [2\pi] \\ \phi_{lm}^{\text{data}}(t) = \phi_{lm}(\mathbf{x}, t) + \varphi_m(t) - \varphi_l(t) + \text{noise} [2\pi] \\ \phi_{mk}^{\text{data}}(t) = \phi_{mk}(\mathbf{x}, t) + \varphi_k(t) - \varphi_m(t) + \text{noise} [2\pi] \end{cases} \quad (9)$$

and the turbulent pistons cancel out in the closure phase defined by :

$$\begin{aligned} \beta_{klm}^{\text{data}}(t) &\triangleq \phi_{kl}^{\text{data}}(t) + \phi_{lm}^{\text{data}}(t) + \phi_{mk}^{\text{data}}(t) + \text{noise} [2\pi] \\ &= \phi_{kl}(\mathbf{x}, t) + \phi_{lm}(\mathbf{x}, t) + \phi_{mk}(\mathbf{x}, t) + \text{noise} [2\pi] \\ &\triangleq \beta_{klm}(\mathbf{x}, t) + \text{noise} [2\pi]. \end{aligned} \quad (10)$$

We have the following properties :

- the set of all three-telescope closure phases that can be formed using a complete array is generated by the  $(N_t - 1)(N_t - 2)/2$  closure phases  $\beta_{1kl}^{\text{data}}(t)$ ,  $k < l$ , *i.e.* the closure phase which include telescope  $T_1$  (indeed,  $\beta_{klm}^{\text{data}} = \beta_{1kl}^{\text{data}} + \beta_{1lm}^{\text{data}} - \beta_{1km}^{\text{data}}$ ). In what follows, these canonical closure phases are grouped together in a vector  $\boldsymbol{\beta}^{\text{data}}$  and  $\mathbf{C}$  denotes the linear closure operator such that  $\mathbf{C}\boldsymbol{\phi}^{\text{data}} = \boldsymbol{\beta}^{\text{data}}$  (see appendix A).
- if  $f$  is a continuous differentiable function verifying property (8), then

$$f(\boldsymbol{\phi}) = g(\mathbf{C}\boldsymbol{\phi}), \quad (11)$$

where  $g$  is some continuous differentiable function. In other terms, there is essentially *no operator other than the closure operator* that cancels out the effect of turbulence on short-exposure visibility phases (this property holds only in the monochromatic case).

The proof of the second property is given in appendix B.

### 2.D. Long-exposure observables data model

To minimize the effect of noise, one is led to average short-exposure measurements, into long-exposure observables, chosen so that they are asymptotically unbiased. The averaging time must be short enough w. r. t. the earth rotation so that the baseline does not change, and long enough to reach an acceptable Signal-to-Noise Ratio (SNR). The averaged quantities are generally:

- averaged *squared amplitudes*  $\mathbf{s}^{\text{data}}(t) = \langle \mathbf{a}^{\text{data}}(t + \tau)^2 \rangle_\tau$ ,
- averaged *bispectra*  $\mathbf{V}_{1kl}^{\text{data}}(t) = \langle y_{1k}^{\text{data}}(t + \tau) \cdot y_{kl}^{\text{data}}(t + \tau) \cdot y_{l1}^{\text{data}}(t + \tau) \rangle_\tau$ ,  $k < l$ .

Squared amplitudes are preferred to amplitudes because their bias can be estimated and subtracted from the data. Short-exposure bispectra are continuous differentiable functions verifying property (8), and so correspond to a particular choice of  $g$  in (11). In absence of noise, the averaged bispectrum amplitudes are redundant with the averaged squared amplitudes. Although they should be useful in low SNR conditions, averaged bispectrum amplitudes are not considered in what follows. The averaged bispectrum phases  $\beta_{1kl}^{\text{data}}(t)$ ,  $k < l$  constitute unbiased long-exposure closure phase estimators. As such, they are linked to the object phases  $\boldsymbol{\phi}(\mathbf{x}, t)$  through:

$$\boldsymbol{\beta}^{\text{data}}(t) = \mathbf{C}\boldsymbol{\phi}(\mathbf{x}, t) + \text{noise} [2\pi] \quad (12)$$

It is shown in appendix A that the kernel of the closure operator  $\mathbf{C}$  is of dimension  $(N_t - 1)$ . Hence equation (12) implies that optical interferometry through turbulence has to deal with a partial phase information. This result can also be obtained by counting up phase unknowns for each instant of measurement  $t$ : there are  $N_t(N_t - 1)/2$  unknown object visibility phases and  $(N_t - 1)(N_t - 2)/2$  observable independent closure phases, which results in  $(N_t - 1)$  missing phase data. As well known in the radio-interferometric community, the more apertures in the array, the smaller the proportion of missing phase information will be.

The long-exposure observables considered in this paper are noisy squared amplitudes  $\mathbf{s}^{\text{data}}(t)$  and closure phases  $\boldsymbol{\beta}^{\text{data}}(t)$ . The only statistics usually available are the variances for each observable (as, for instance, in the OIFITS data exchange format [11]). The assumed noise distribution is

consequently 0-mean white Gaussian:

$$\begin{cases} \mathbf{s}^{\text{data}}(t) = \mathbf{a}^2(\mathbf{x}, t) + \mathbf{s}^{\text{noise}}(t), & \mathbf{s}^{\text{noise}}(t) \sim \mathcal{N}(\mathbf{0}, \mathbf{R}_{\mathbf{s}(t)}) \\ \boldsymbol{\beta}^{\text{data}}(t) = \mathbf{C}\boldsymbol{\phi}(\mathbf{x}, t) + \boldsymbol{\beta}^{\text{noise}}(t) [2\pi], & \boldsymbol{\beta}^{\text{noise}}(t) \sim \mathcal{N}(\mathbf{0}, \mathbf{R}_{\boldsymbol{\beta}(t)}) \end{cases} \quad (13)$$

The matrices  $\mathbf{R}_{\mathbf{s}(t)}$  and  $\mathbf{R}_{\boldsymbol{\beta}(t)}$  are diagonal, with variances related to the integration time, although correlations may be produced by the use of the same reference stars in the calibration process<sup>12</sup>.

## 2.E. Bayesian reconstruction methods

This approach first forms the anti-log-likelihood according to the model (13)

$$J^{\text{data}}(\mathbf{x}) = \sum_t J^{\text{data}}(\mathbf{x}, t) = \sum_t \chi_{\mathbf{s}(t)}^2(\mathbf{x}) + \chi_{\boldsymbol{\beta}(t)}^2(\mathbf{x}) \quad (14)$$

where  $\chi_{\mathbf{s}(t)}^2(\mathbf{x})$  denotes the  $\chi^2$  statistic  $(\mathbf{s}^{\text{data}}(t) - \mathbf{a}^2(\mathbf{x}, t))^{\text{T}} \mathbf{R}_{\mathbf{s}(t)}^{-1} (\mathbf{s}^{\text{data}}(t) - \mathbf{a}^2(\mathbf{x}, t))$ . Closure terms  $\chi_{\boldsymbol{\beta}(t)}^2(\mathbf{x})$  are a weighted quadratic distance between complex phasors<sup>13</sup> instead of a Chi-2 statistic over closure phase residuals. One then associates  $J^{\text{data}}$  with a regularization term to account for the incompleteness of the data in such inverse problems and minimizes the composite criterion

$$J(\mathbf{x}) = J^{\text{data}}(\mathbf{x}) + J^{\text{prior}}(\mathbf{x}) \quad (15)$$

under the following constraints:

$$\begin{aligned} \forall(p, q), x(p, q) &\geq 0 \\ \sum_{p, q} x(p, q) &= 1. \end{aligned} \quad (16)$$

The first requires positivity of the sought object, the second is a constraint of unit flux. Indeed, fringe visibilities are by definition flux-normalized quantities (*i.e.* normalized by the Fourier transform of the object at the null frequency, see Eq. 3), so the data are independent of the total flux of the sought object (of course an interferometer is sensitive to the total flux of the source, but this last value is not contained in the fringe visibility itself).

The regularization term  $J^{\text{prior}}$  is chosen to enforce some properties of the object which are known a priori (smoothness, spiky behavior, positivity, etc.) and should also ease the minimization. Simple and popular regularization terms are convex separable penalizations of the object pixels (*i.e.* *white priors*) or of the object spatial derivatives (for instance first-order derivative or gradient). In what follows, we quickly describe the prior terms used in this paper. These priors are more extensively described and compared in [14]. For a general review on regularization, see [15].

Entropic priors belong to the family of white priors and often allow to obtain a clean image while preserving its sharp spiky features, whereas quadratic penalization tends to soften the reconstructed map. The white quadratic-linear (or  $L_2L_1^w$ ) penalization given by:

$$L_2L_1^w(\mathbf{x}) = \delta^2 \sum_{p, q} \frac{\mathbf{x}(p, q)}{s\delta} - \ln \left( 1 + \frac{\mathbf{x}(p, q)}{s\delta} \right) \quad (17)$$

that we use in section 5 leads to a kind of entropic regularization, in the sense of [16]. We propose a nominal setting of the two parameters  $\delta$  and  $s$ :

$$s = 1/N_{\text{pix}}; \quad \delta = 1. \quad (18)$$

As regards regularization based on the object's spatial derivatives, we shall consider here only quadratic penalization, but convex quadratic-linear  $L_2L_1$  penalization functions could also be invoked.

Ref. [17] is one of the works that adopt such a Bayesian approach for processing optical long baseline interferometry, using a constrained local descent method to minimize (15). A convex data criterion  $J$ , i.e. such that  $J(k \cdot x_1 + (1 - k) \cdot x_2) \leq k \cdot J(x_1) + (1 - k) \cdot J(x_2)$ ,  $\forall x_1, x_2, \forall k \in [0, 1]$ , has no local minima, which makes the minimization much easier. Unfortunately, the criterion  $J$  is non-convex. To be more precise, the difficulty of the problem can be summed up as follows:

- (i) The small number of Fourier coefficients makes the problem under-determined. Here the regularization term and the positivity constraint can help by limiting the high frequencies of the reconstructed object [6].
- (ii) Closure phase measurements implies missing phase information and makes the Fourier synthesis problem non-convex. Adding a regularization term does not generally correct the problem [18].
- (iii) Phase and modulus measurements with additive Gaussian noise leads to a non-Gaussian likelihood and a non-convex log-likelihood w.r.t.  $\mathbf{x}$ . As a consequence, even with no missing phases, some approximation of the real observable statistics is necessary to get a convex data fidelity term. This data conversion from polar to Cartesian coordinates, which is commonly used in the field of radar processing [19], has been studied only recently in OLBI [20]: see section 3.C.

These characteristics imply that optimizing  $J$  by a local descent algorithm can only work if the initialization selects the "right" valley of the criterion. The design of a good initial position is very case-dependent, and will not be extensively addressed here. The other key aspects are then the followed path, i.e. the minimization method, and the shape of the function to minimize, i.e. the behavior of the criterion  $\mathbf{x} \mapsto J(\mathbf{x})$ . This paper addresses both aspects:

- we design a specific OLBI criterion  $\mathcal{J}(\mathbf{x}, \boldsymbol{\alpha})$  where two sets of variables appear explicitly, one in the spatial domain  $\mathbf{x}$ , describing the sought object, and another in the Fourier phase domain  $\boldsymbol{\alpha}$ , which accounts for the missing phase information. This specific criterion is designed to solve (iii), i.e. so that for a known  $\boldsymbol{\alpha}$ , the criterion is convex w. r. t.  $\mathbf{x}$ . In other words, if we had all the complex visibility phase measurements instead of just the closure phases, our criterion  $\mathbf{x} \mapsto \mathcal{J}(\mathbf{x}, \boldsymbol{\alpha})$  would be convex;
- we adopt an alternate minimization method, working on the two sets of variables.

This approach can be related to "myopic" approaches of some inverse problems, where missing data concerning the instrumental response are modeled and sought for during the inversion [21]. Alternate minimization methods are inspired by self-calibration methods in radio-interferometry, and have been used in optical interferometry by Lannes et al. [6]. However, the criterion used in

Ref. [6] was essentially imported from radio-interferometry and does not match the OLBI data model (13). Our main contribution is to derive a criterion which accounts for the data model (13), while allowing an efficient alternate minimization. This construction is the subject of the next section.

### 3. An equivalent myopic model for self-calibration

The aim of this section is to approximate the data model of equation (13):

$$\mathbf{s}^{\text{data}}(t) = \mathbf{a}^2(\mathbf{x}, t) + \mathbf{s}^{\text{noise}}(t), \quad \mathbf{s}^{\text{noise}}(t) \sim \mathcal{N}(\mathbf{0}, \mathbf{R}_{\mathbf{s}(t)}) \quad (19)$$

$$\beta^{\text{data}}(t) = \mathbf{C}\phi(\mathbf{x}, t) + \beta^{\text{noise}}(t) [2\pi], \quad \beta^{\text{noise}}(t) \sim \mathcal{N}(\mathbf{0}, \mathbf{R}_{\beta(t)}) \quad (20)$$

by a myopic linear model with additive complex Gaussian noise of the following form:

$$\mathbf{y}^{\text{data}}(t) = \mathcal{F}_{\alpha(t)} \cdot \mathbf{H}(t)\mathbf{x} + \mathbf{y}^{\text{noise}}(t) \quad (21)$$

where operator  $\cdot$  denotes componentwise multiplication, and  $\mathcal{F}_{\alpha(t)}$  is a vector of phasors depending on phase aberration parameters  $\alpha(t)$ , which are defined in Sec. 3.B. This will be done in three steps:

- Sec. 3.A is devoted to the derivation of the observation model for the pseudo amplitude term  $\mathbf{a}^{\text{data}}(t)$  from (19);
- Sec. 3.B is devoted to the derivation of the observation model for the pseudo phase term  $\phi^{\text{data}}(t)$  from (20);
- Sec. 3.C shows how to combine pseudo phase and pseudo amplitude models in a complex model such as equation (21) while solving problem (iii) of Sec. 2.E.

#### 3.A. Pseudo amplitude data model

In Eq. (19), we have supposed a Gaussian distribution for  $\mathbf{s}^{\text{data}}(t)$  around  $\mathbf{s}(\mathbf{x}, t)$ , which is questionable, since squared amplitudes should be non-negative. However, such a statistic model is acceptable provided that the probability of a negative component of  $\mathbf{s}^{\text{data}}(t)$  is very weak. For uncorrelated measurements, this assumption correspond to mean values much greater than the corresponding standard deviation. Appendix D page 19 shows how to build the mean and covariance matrix of the square root of such a distribution. The mean vector is taken as the pseudo amplitude data  $\mathbf{a}^{\text{data}}(t)$ , and the covariance matrix called  $\mathbf{R}_{\mathbf{a}(t)}$ .

The observation model (19) can then be approximated by the following amplitude pseudo data model:

$$\mathbf{a}^{\text{data}}(t) = \mathbf{a}(\mathbf{x}, t) + \mathbf{a}^{\text{noise}}(t), \quad \mathbf{a}^{\text{noise}}(t) \sim \mathcal{N}(\mathbf{0}, \mathbf{R}_{\mathbf{a}(t)}) . \quad (22)$$

#### 3.B. Pseudo phase data model

We start from a generalized inverse solution to the phase closure equation of (20). The generalized inverse  $\mathbf{C}^\dagger$  of  $\mathbf{C}$ , defined by  $\mathbf{C}^\dagger \triangleq \mathbf{C}^T [\mathbf{C}\mathbf{C}^T]^{-1}$ , is such that  $\mathbf{C}\mathbf{C}^\dagger = \mathbf{Id}$ . By applying it on all the terms of (20), we obtain

$$\mathbf{C}^\dagger \beta^{\text{data}}(t) = \mathbf{C}^\dagger \mathbf{C}\phi(\mathbf{x}, t) + \mathbf{C}^\dagger \beta^{\text{noise}}(t) + 2\pi \mathbf{C}^\dagger \boldsymbol{\kappa} \quad (23)$$



where  $\boldsymbol{\kappa}$  is a vector of integers to account for the fact that each phase component is measured modulo  $2\pi$ . We define

$$\boldsymbol{\phi}^{\text{data}}(t) \triangleq \mathbf{C}^\dagger \boldsymbol{\beta}^{\text{data}}(t) \quad (24)$$

$$\boldsymbol{\phi}^{\text{ker}}(t) \triangleq (\mathbf{C}^\dagger \mathbf{C} - \mathbf{Id}) \boldsymbol{\phi}(\mathbf{x}, t) + 2\pi \mathbf{C}^\dagger \boldsymbol{\kappa} \quad (25)$$

and obtain

$$\boldsymbol{\phi}^{\text{data}}(t) = \boldsymbol{\phi}(\mathbf{x}, t) + \boldsymbol{\phi}^{\text{ker}}(t) + \mathbf{C}^\dagger \boldsymbol{\beta}^{\text{noise}}(t) \quad (26)$$

Vector  $\boldsymbol{\phi}^{\text{ker}}(t)$  belongs to the  $2\pi$ -wrapped kernel of operator  $\mathbf{C}$  :

$$\begin{aligned} \mathbf{C} \boldsymbol{\phi}^{\text{ker}}(t) &= (\underbrace{\mathbf{C} \mathbf{C}^\dagger \mathbf{C}}_{=\mathbf{Id}} - \mathbf{C}) \boldsymbol{\phi}(\mathbf{x}, t) + 2\pi \underbrace{\mathbf{C} \mathbf{C}^\dagger}_{=\mathbf{Id}} \boldsymbol{\kappa} \\ &= 2\boldsymbol{\kappa} \pi \\ &= \mathbf{0} [2\pi] \end{aligned}$$

As shown in appendix C, if  $\boldsymbol{\phi}^{\text{ker}} = \mathbf{0} [2\pi]$ , there exists a real vector  $\boldsymbol{\alpha}(t)$  of dimension  $N_t - 1$  such that  $\boldsymbol{\phi}^{\text{ker}}(t) = \bar{\mathbf{B}} \boldsymbol{\alpha}(t) [2\pi]$ , where  $\bar{\mathbf{B}}$  is obtained by removing the first column of operator  $\mathbf{B}$ . So we have:

$$\boldsymbol{\phi}^{\text{data}}(t) = \boldsymbol{\phi}(\mathbf{x}, t) + \bar{\mathbf{B}} \boldsymbol{\alpha}(t) + \mathbf{C}^\dagger \boldsymbol{\beta}^{\text{noise}}(t) [2\pi] \quad (27)$$

Now the problem is that  $\mathbf{C}^\dagger \boldsymbol{\beta}^{\text{noise}}(t)$  is a zero mean random vector with a *singular covariance matrix*

$$\mathbf{R}_{\boldsymbol{\phi}(t)}^0 \triangleq \mathbf{C}^\dagger \mathbf{R}_{\boldsymbol{\beta}(t)} \mathbf{C}^{\dagger T}.$$

To obtain a strictly convex log-likelihood, we have to approximate this term by a proper Gaussian vector  $\boldsymbol{\phi}^{\text{noise}}(t)$ , with an invertible covariance matrix  $\mathbf{R}_{\boldsymbol{\phi}(t)}$  chosen so as to correctly fit the second order statistics of the noise in the phase closure measurement equation (20). This last requirement can be written as the following equation:

$$\mathbf{C} \mathbf{R}_{\boldsymbol{\phi}(t)} \mathbf{C}^T = \mathbf{R}_{\boldsymbol{\beta}(t)}. \quad (28)$$

In other words, we are led to choose an invertible covariance matrix  $\mathbf{R}_{\boldsymbol{\phi}(t)}$  so as to mimic the statistical behavior of the closures, which is expressed by (28).

We propose to modify matrix  $\mathbf{R}_{\boldsymbol{\phi}(t)}^0$  by setting its non diagonal components to 0, *i.e.* to use the following diagonal matrix:

$$\{\mathbf{R}_{\boldsymbol{\phi}(t)}\}_{ij} = \begin{cases} 3 \cdot \{\mathbf{R}_{\boldsymbol{\phi}(t)}^0\}_{ij} & \text{if } i = j \\ 0 & \text{if } i \neq j \end{cases}. \quad (29)$$

The factor 3 allows us to preserve the total weight of the phase term in the log-likelihood by satisfying the condition:

$$\sum_{i,j} |\{\mathbf{R}_{\boldsymbol{\phi}(t)}\}_{ij}| = \sum_{i,j} |\{\mathbf{R}_{\boldsymbol{\phi}(t)}^0\}_{ij}|.$$

There are several ways of choosing  $\mathbf{R}_{\boldsymbol{\phi}(t)}$ , and we propose this particular choice without claiming it is optimal. Note that the myopic model derived in what follows can accommodate to any choice of a proper (*i.e.* invertible) covariance matrix  $\mathbf{R}_{\boldsymbol{\phi}(t)}$ .

With equations (24), (27) and (29), we obtain the visibility phase pseudo data model:

$$\boldsymbol{\phi}^{\text{data}}(t) = \boldsymbol{\phi}(\mathbf{x}, t) + \bar{\mathbf{B}} \boldsymbol{\alpha}(t) + \boldsymbol{\phi}^{\text{noise}}(t) [2\pi], \quad \boldsymbol{\phi}^{\text{noise}}(t) \sim \mathcal{N}(\mathbf{0}, \mathbf{R}_{\boldsymbol{\phi}(t)}). \quad (30)$$

### 3.C. Pseudo complex visibility data model

Gathering equations (22) and (30), we have finally approximated the data model (19-20) by

$$\begin{cases} \mathbf{a}^{\text{data}}(t) = \mathbf{a}(\mathbf{x}, t) + \mathbf{a}^{\text{noise}}(t), & \mathbf{a}^{\text{noise}}(t) \sim \mathcal{N}(\mathbf{0}, \mathbf{R}_{\mathbf{a}(t)}) \\ \phi^{\text{data}}(t) = \phi(\mathbf{x}, t) + \bar{\mathbf{B}}\boldsymbol{\alpha}(t) + \phi^{\text{noise}}(t) [2\pi], & \phi^{\text{noise}}(t) \sim \mathcal{N}(\mathbf{0}, \mathbf{R}_{\phi(t)}) \end{cases} \quad (31)$$

We form pseudo-complex visibility measurements  $\mathbf{y}^{\text{data}}(t)$  defined by:

$$\mathbf{y}^{\text{data}}(t) \triangleq \mathbf{a}^{\text{data}}(t) \cdot e^{i\phi^{\text{data}}(t)}. \quad (32)$$

The approach proposed in [20], which we recall and generalize in Appendix E, is based on an approximated complex visibility data model

$$\mathbf{y}^{\text{data}}(t) = \mathbf{H}(t)\mathbf{x} \cdot e^{i\bar{\mathbf{B}}\boldsymbol{\alpha}(t)} + \mathbf{y}^{\text{noise}}(t) \quad (33)$$

This is exactly the sought model stated the beginning of the present section in equation (21), with  $\mathcal{F}_{\boldsymbol{\alpha}(t)} = e^{i\bar{\mathbf{B}}\boldsymbol{\alpha}(t)}$ . We now define the myopic observation model as follows:

$$\mathbf{y}_m(\mathbf{x}, \boldsymbol{\alpha}(t)) \triangleq \mathbf{H}(t)\mathbf{x} \cdot e^{i\bar{\mathbf{B}}\boldsymbol{\alpha}(t)}. \quad (34)$$

As shown in Appendix E, the mean value  $\bar{\mathbf{y}}^{\text{noise}}(t)$  and covariance matrix  $\mathbf{R}_{\mathbf{y}^{\text{noise}}(t)}$  of the additive complex noise term  $\mathbf{y}^{\text{noise}}(t)$  are carefully designed so that the corresponding data likelihood criterion is convex quadratic w. r. t. the complex  $\mathbf{y}_m(\mathbf{x}, \boldsymbol{\alpha}(t))$  while remaining close to the real non convex model. To illustrate these properties, we consider one complex visibility and plot in the complex plane the distribution of  $\mathbf{y}^{\text{data}}(t)$  around  $\mathbf{y}_m(\mathbf{x}, \boldsymbol{\alpha}(t))$  for the true noise distribution — i.e. a polar Gaussian noise in phase and modulus — and our cartesian Gaussian approximation (see Fig. 1) In particular, the “elliptic” covariance matrix we propose (which yields elliptic contour plots in Fig. 1), is preferable to the more classical “circular” approximation that appears in previous contributions on OLBI [22]. The latter can be described by half as many parameters as needed for the elliptic one (one radius for a circle, instead of a short axis and a long axis for an ellipsis), but is clearly less accurate [20] (such a noise statistics description has also been investigated for the complex bispectra in the OIFITS data exchange format [11]).

From Eq. (33), we build a Chi-2 statistics over real and imaginary parts of the observation equation

$$\chi_{\mathbf{y}(t)}^2(\mathbf{x}, \boldsymbol{\alpha}(t)) \triangleq \begin{bmatrix} \Re \{ \mathbf{y}^{\text{data}}(t) - \mathbf{y}_m(\mathbf{x}, \boldsymbol{\alpha}(t)) - \bar{\mathbf{y}}^{\text{noise}}(t) \} \\ \Im \{ \mathbf{y}^{\text{data}}(t) - \mathbf{y}_m(\mathbf{x}, \boldsymbol{\alpha}(t)) - \bar{\mathbf{y}}^{\text{noise}}(t) \} \end{bmatrix}^T \times \mathbf{R}_{\mathbf{y}^{\text{noise}}(t)}^{-1} \begin{bmatrix} \Re \{ \mathbf{y}^{\text{data}}(t) - \mathbf{y}_m(\mathbf{x}, \boldsymbol{\alpha}(t)) - \bar{\mathbf{y}}^{\text{noise}}(t) \} \\ \Im \{ \mathbf{y}^{\text{data}}(t) - \mathbf{y}_m(\mathbf{x}, \boldsymbol{\alpha}(t)) - \bar{\mathbf{y}}^{\text{noise}}(t) \} \end{bmatrix}.$$

And we finally propose the myopic goodness-of-fit criterion:

$$\mathcal{J}^{\text{data}}(\mathbf{x}, \boldsymbol{\alpha}) = \sum_t \mathcal{J}^{\text{data}}(\mathbf{x}, \boldsymbol{\alpha}(t), t) = \sum_t \chi_{\mathbf{y}(t)}^2(\mathbf{x}, \boldsymbol{\alpha}(t)) \quad (35)$$

We can now design a myopic Bayesian approach to the reconstruction problem, by combining the data term with a regularization term along the lines of Section 2.E:

$$\mathcal{J}(\mathbf{x}, \boldsymbol{\alpha}) = \mathcal{J}^{\text{data}}(\mathbf{x}, \boldsymbol{\alpha}) + J^{\text{prior}}(\mathbf{x}). \quad (36)$$

The next section describes an alternate minimization technique applied to the regularized criterion (36).

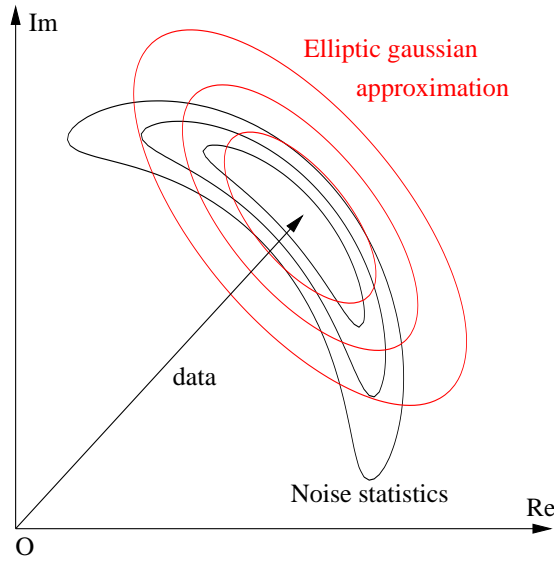


Fig. 1. Contour plots of a polar Gaussian distribution and of its Cartesian Gaussian approximation

#### 4. WISARD

In this section, we describe WISARD, standing for Weak-phase Interferometric Sample Alternating Reconstruction Device, a self-calibration method for OLBII.

##### 4.A. Global structure of WISARD

WISARD is made of four major blocks:

- a first block recasts the raw data (i.e. closure phases and squared visibilities) in myopic data (i.e. phases and moduli) as described in sections 3.A and 3.B;
- a second "convexification block" computes a Gaussian approximation of the pseudo visibility data model as described in section 3.C;
- a third block builds a guess for the object  $x$  and aberrations  $\alpha$  (i.e. a good starting point);
- finally, the self-calibration block performs the minimization of the regularized criterion (36), under the constraints (16). It alternates optimization of the object for given aberrations, and optimization of the aberrations for the current object.

The structure of WISARD is sketched in Fig. 2. The principles which underline the three first blocks of WISARD have been described in previous Sections, while details on the self-calibration minimization are gathered in the next one.

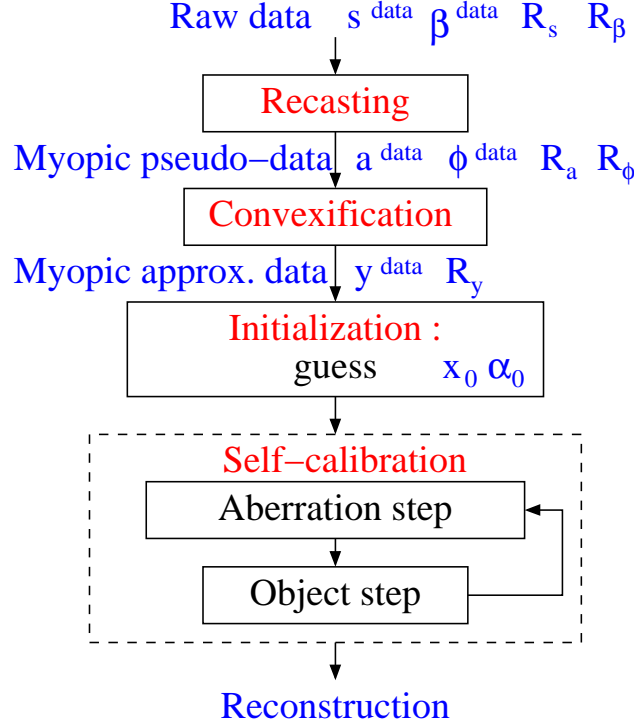


Fig. 2. WISARD algorithm loop

#### 4.B. Self-calibration block

**Minimization w. r. t.  $\mathbf{x}$**  The criterion  $\mathcal{J}^{\text{data}}(\mathbf{x}, \boldsymbol{\alpha})$  we have derived is quadratic hence convex w.r.t. the object  $\mathbf{x}$ . Hence, the minimization versus  $\mathbf{x}$  does not raise special difficulties.

**Minimization w. r. t.  $\boldsymbol{\alpha}$**   $\mathcal{J}^{\text{data}}(\mathbf{x}, \boldsymbol{\alpha})$  is the sum of terms involving only measurements obtained at one time instant  $t$  (equation 35):

$$\mathcal{J}^{\text{data}}(\mathbf{x}, \boldsymbol{\alpha}) = \sum_t \mathcal{J}^{\text{data}}(\mathbf{x}, \boldsymbol{\alpha}(t), t)$$

Because the time between two measurements is much greater than the turbulence coherent time (around 10 ms), aberrations  $\boldsymbol{\alpha}(t)$  at two different instants are statistically independent. We can then solve separately for each set of  $\boldsymbol{\alpha}(t)$ , which dramatically reduces the complexity of the minimization. The number of  $\boldsymbol{\alpha}(t)$  components to solve for is  $(N_t - 1)$  and the minimization is delicate, as the criterion exhibits periodic structures which have been studied in [22].

However, exact minimization is affordable for a 3-telescope interferometric array. In this case we have to perform several 2-parameter minimizations, and each one can be efficiently initialized by an exhaustive search on a 2-D grid, which ensures we avoid local minima. On the other hand, when  $N_t$  gets high enough, *e.g.* 6, then number of  $\boldsymbol{\alpha}(t)$  to solve for, *e.g.* 5, gets small compared to the number of closure phases available, *e.g.* 15. With a 3-telescope array, 2/3 of the phase information is missing, whereas with a 6-telescope array, only 1/3 of the phase information is missing.

In this last case, which corresponds to the processing of synthetic data presented Sec. 5.A, the reconstructions were straightforward, and no effects of the local minima in  $\alpha$  were witnessed.

In other words, coping with the ambiguities in  $\alpha$ , for instance with the specific criterion proposed in [22], may be necessary only for  $N_t = 4$  or  $N_t = 5$ . For  $N_t = 3$ , an exhaustive search is possible, and for  $N_t \geq 6$ , ambiguities in  $\alpha$  do not have, according to our experience, a major impact on reconstruction.

**Starting point : object and aberration guess  $x_0$  and  $\alpha_0$**  If a parametric model of the observed stellar source is not available, the object starting point is a mean square solution, from which we extract the positive part. The first step in the self-calibration block is a minimization w. r. t.  $\alpha$  for  $x = x_0$ .

## 5. Results

This section presents some results of processing by the WISARD algorithm, with both synthetic and experimental data.

### 5.A. Processing of synthetic data

The first example takes synthetic interferometric data that were used in the international Imaging Beauty Contest organized by P. Lawson for the IAU [23]. These data simulate the observation of the synthetic object shown in figure 3 with the NPOI [24] 6-telescope interferometer. The corresponding frequency coverage, shown in figure 3, has a structure in arcs of circles typical of the *super-synthesis* technique, which consists in repeating the measurements over several nights of observation so that the same baselines access different measurement spatial frequencies because of the Earth's rotation. In total, there are 195 square visibility modules and 130 closure phases, together with the associated variances.

Six reconstructions obtained with WISARD are shown in figure 4. On the upper row is a reconstruction using a quadratic regularization based on a power spectral density model in  $1/|u|^3$ , for a weak, a strong and a correct regularization parameter. The latter gives a satisfactory level of smoothing but does not restore the peak in the center of the object. The peak is visible in the under-regularized reconstruction on the left but at the cost of too high a residual variance.

The reconstruction presented on the lower row is a good trade-off between smoothing and restoration of the central peak thanks to the use of the white  $L_2L_1^w$  prior term introduced in section 2.E. The automatically set parameters (eq. 18) are very satisfactory (left), and a light tuning (center and right) allow an even better reconstruction. The goodness of fit of the  $L_2L_1^w$  reconstruction can be appreciated in figure 5. The red crosses show the reconstructed visibility moduli (i.e. of the FT of the reconstructed object at the measurement frequencies) and the blue squares are the moduli of the measured visibilities. The difference between the two, weighted by 10 times the standard deviation of the moduli, is shown as the dotted line. The mean value of this difference is 0.1, which shows a good fit (to within  $1 \sigma$ ).

### 5.B. Processing of experimental data

Here, we present the reconstruction the star  $\chi$  Cygni from experimental data using the WISARD algorithm. The data were obtained by S. Lacour and S. Meimon under the leadership of G. Perrin during a measuring campaign on the IOTA interferometer [25] in May 2005. As already mentioned,

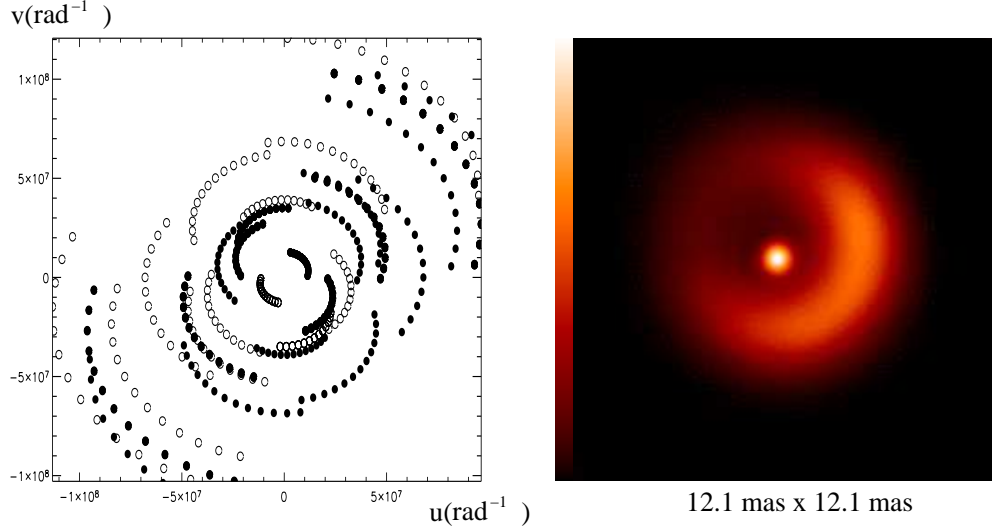


Fig. 3. Synthetic object (right) and frequency coverage (left) from the Imaging Beauty Contest 2004

each measurement has to be calibrated by observation of an object that acts as a point source at the instrument's resolving power. The calibrators chosen were HD 180450 and HD 176670.

$\chi$  Cygni is a Mira-type star, Mira itself being an example of such stars. Perrin et al. [26] propose a model of Mira-type stars, composed of a photosphere, an empty layer, and a thin molecular layer. The aim of the mission was to obtain images of  $\chi$  Cygni in the H band (1.65 microns  $\pm 175nm$ ) and, in particular, to highlight possible asymmetric features in the structure of the molecular layer.

Figure 6 shows, on the left, the  $u - v$  coverage obtained, i.e. the set of spatial frequencies measured, multiplied by the observation wavelength. Because the sky is habitually represented with the west on the right, the coordinates used are, in fact,  $-u, v$ . The domain of the accessible  $u - v$  plane is constrained by the geometry of the interferometer and the position of the star in the sky. The "hour-glass" shape is characteristic of the IOTA interferometer, and entails non-uniform resolution that affects the image reconstruction, shown on the right. The reconstructed angular field has sides of 60 milliarcseconds. In addition to the positivity constraint, the regularization term used is the  $L_2L_1^w$  term described in section 2.E. The interested reader will find an astrophysical interpretation of this result in [27].

## 6. Concluding comments

We have proposed a complete and precise self-calibration approach to optical interferometry image reconstruction. After pointing out the data model specificities in the optical long baseline interferometry context, we have emphasized the sources of under-determinations, which make a classical Bayesian criterion descent method critical. Namely, the main problems are the phase under-determination caused by turbulence effects, and, as noted only recently, the polar coordinate structure of the data model.

We have built a specially-designed approximate myopic data-model, in order to derive a self

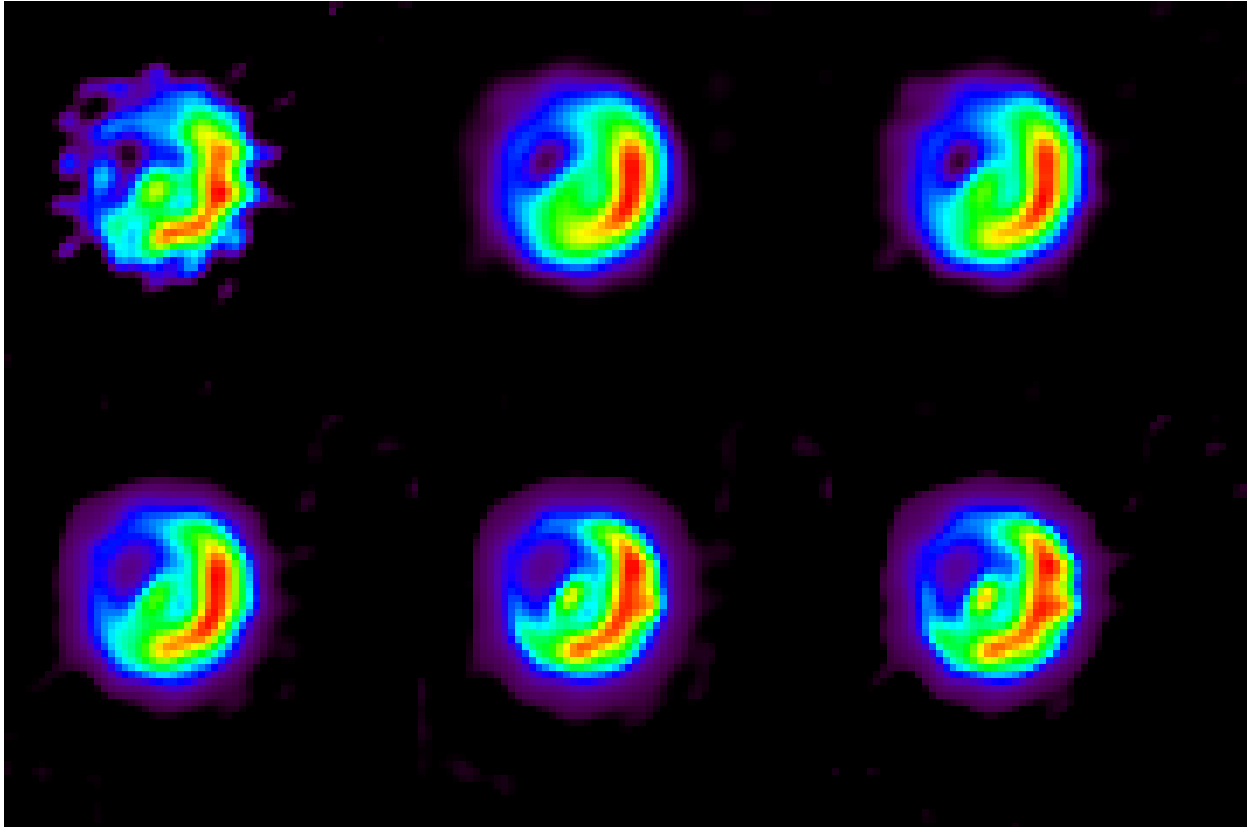


Fig. 4. Reconstructions with WISARD. Upper row : under-regularized quadratic model (left), over-regularized quadratic model (center), quadratic model with correct regularization parameter (right). Lower row : white  $L_2L_1^w$  model with automatically set scale and delta parameters (left), white  $L_2L_1^w$  model with half scale (center), white  $L_2L_1^w$  model with half delta (right). Each image field is  $12.1 \times 12.1$  mas.

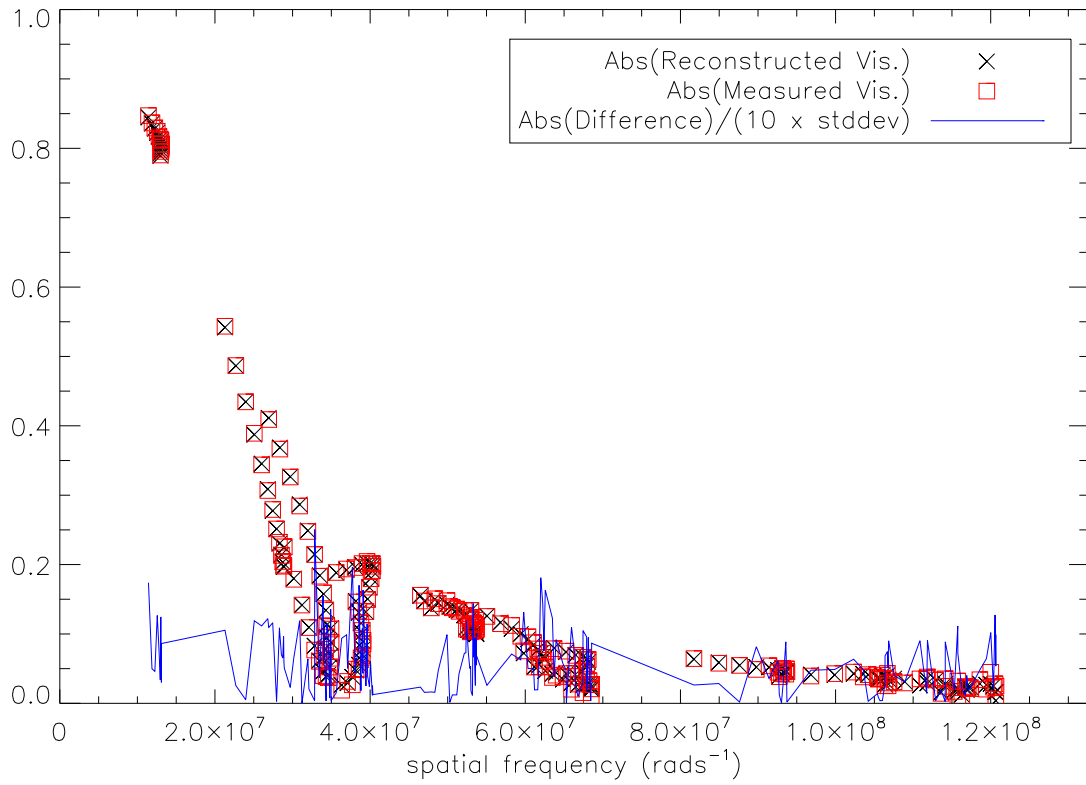


Fig. 5. Goodness of fit at WISARD convergence.

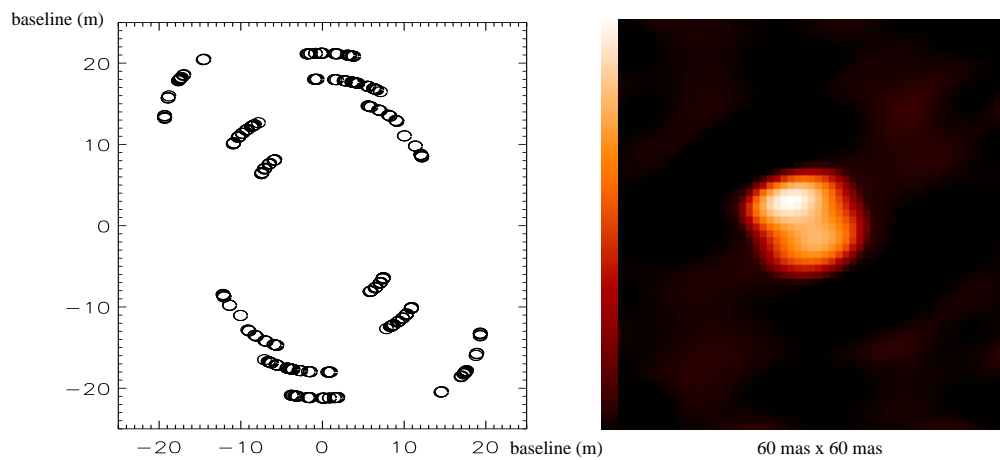


Fig. 6. Frequency coverage (left) and reconstruction of the star  $\chi$  Cygni (right).



calibration method. Special care was given to the design of the second order statistics of the myopic model, an aspect which was ignored in previous related works.

We have extended our previous work on polar data conversion<sup>20</sup> and proposed a convex approximation of the noise model which reduces the number of local minima of the criterion to minimize.

We also addressed integer ambiguities induced by closure phase wrapping, which are classical when dealing with phase data, and have discussed their impact on the image reconstruction quality : for 3 telescope data, we have proposed an exhaustive search method, and we have witnessed that these ambiguities do not raise any particular problem when processing 6 or more telescope interferometer data. Concerning the remaining 4-5 telescope case, the work by Lannes [22] should be worth investigating. On the other hand, global minimization methods were left aside because of their intensive computation needs. As computer performance increases, these methods might be, in the years to come, an appropriate way to deal with local minima.

All these developments allowed us to propose WISARD, a self-calibration method for optical long baseline interferometry image reconstruction, and to demonstrate its efficiency on simulated data.

Finally WISARD was also used to successfully process real astronomical OLBI datasets. These results were made possible thanks to a close partnership with the astronomers Sylvestre Lacour and Guy Perrin of the Observatoire de Paris Meudon, within the PHASE group (ONERA/LESIA). Indeed, an accurate astronomical model of the observed stellar object is a precious guideline for reconstructing a complex image from optical long baseline interferometric data. To the authors point of view, such a collaboration is essential to the success of OLBII techniques.

## A. The baseline and closure operators $C$ and $B$

Let  $N_t$  be the number of telescopes of the interferometric array. We have the following definitions:

$$\mathbf{B}_2 \triangleq \begin{bmatrix} -1 & 1 \end{bmatrix} \quad (37)$$

$$\mathbf{B}_{N_t} \triangleq \left[ \begin{array}{c|c} -\mathbf{1}_{N_t-1} & \mathbf{Id}_{N_t-1} \\ \hline \mathbf{O} & \mathbf{B}_{N_t-1} \end{array} \right] \quad (38)$$

$$\mathbf{C}_{N_t} \triangleq \left[ \begin{array}{c|c} -\mathbf{B}_{N_t-1} & \mathbf{Id}_{\frac{(N_t-1)(N_t-2)}{2}} \end{array} \right] \quad (39)$$

for  $N_t \geq 3$ .

In what follows, we prove that  $\ker \mathbf{C} = \text{im } \mathbf{B}$ .

We have  $\mathbf{C}_{N_t} \mathbf{B}_{N_t} = \mathbf{0}$ , so

$$\text{im } \mathbf{B} \subset \ker \mathbf{C} \quad (40)$$

It is straightforward to prove by recurrence that  $\mathbf{B}_{N_t} \cdot \mathbf{1}_{N_t} = \mathbf{0}$ , which yields  $\text{rank } \mathbf{B}_{N_t} \leq N_t - 1$ . Because  $\mathbf{B}_{N_t}$  contains  $\mathbf{Id}_{N_t-1}$  we gather:

$$\dim \text{im } \mathbf{B} \triangleq \text{rank } \mathbf{B} = N_t - 1. \quad (41)$$

$\mathbf{C}_{N_t}$  contains  $\mathbf{Id}_{\frac{(N_t-1)(N_t-2)}{2}}$ , which yields  $\text{rank } \mathbf{C}_{N_t} \geq \frac{(N_t-1)(N_t-2)}{2}$ , or

$$\dim \ker \mathbf{C}_{N_t} \leq N_t - 1 \quad (42)$$

With (40), (41) and (42), we gather:

$$\ker \mathbf{C} = \text{im } \mathbf{B} \quad (43)$$

## B. Characterization of the baseline phase independent operators

Here, we prove that any continuous differentiable function  $f$  verifying property 8

$$f(\phi + \mathbf{B}\varphi) = f(\phi), \forall(\phi, \varphi)$$

is such that  $f(\phi) = g(\mathbf{C}\phi)$ .  $\mathbf{C}$  has more columns than rows, so its pseudo-inverse is defined by  $\mathbf{C}^\dagger \triangleq \mathbf{C}^T [\mathbf{C}\mathbf{C}^T]^{-1}$  and verifies

$$\mathbf{C}\mathbf{C}^\dagger = \mathbf{Id} \quad (44)$$

and thus

$$\begin{aligned} \mathbf{C}\mathbf{C}^\dagger\mathbf{C} - \mathbf{C} = 0 &\Rightarrow \mathbf{C}(\mathbf{C}^\dagger\mathbf{C}\phi - \phi) = 0, \forall\phi \\ &\stackrel{(43)}{\Rightarrow} \exists\varphi, (\mathbf{C}^\dagger\mathbf{C}\phi - \phi) = \mathbf{B}\varphi, \forall\phi \\ &\Rightarrow \exists\varphi, \phi = \mathbf{C}^\dagger\mathbf{C}\phi - \mathbf{B}\varphi, \forall\phi \end{aligned}$$

With this we obtain that any  $f$  verifying 8 is such that

$$f(\phi) = f(\mathbf{C}^\dagger\mathbf{C}\phi - \mathbf{B}\varphi) = f(\mathbf{C}^\dagger\mathbf{C}\phi) = g(\mathbf{C}\phi).$$

## C. Wrapped kernel of operator $\mathbf{C}$

The kernel of operator  $\mathbf{C}$  is given by  $\ker \mathbf{C} = \text{im } \mathbf{B}$  (equation 43). With dimensional arguments, it is easy to see that

$$\text{im } \mathbf{B} = \text{im } \bar{\mathbf{B}}$$

where  $\bar{\mathbf{B}}$  is obtained by removing the first column of operator  $\mathbf{B}$ , so we have

$$\ker \mathbf{C} = \text{im } \bar{\mathbf{B}} \quad (45)$$

Let us now characterize the set of  $\phi^{\ker}$  such that :

$$\mathbf{C}\phi^{\ker} \equiv 0 [2\pi]$$

Because  $\mathbf{C}$  has integer components,  $\phi^{\ker}$  can be considered modulo  $2\pi$ . With equation 45, we obtain:

$$\exists\alpha_1, \phi^{\ker} \equiv \mathbf{C}^\dagger(0 [2\pi]) + \bar{\mathbf{B}}\alpha_1 [2\pi] \quad (46)$$

Because  $\bar{\mathbf{B}}$  has integer components,  $\alpha_1$  can be considered modulo  $2\pi$ . The issue here is to evaluate the  $\mathbf{C}^\dagger(0 [2\pi])$  term, i.e. the value of  $\mathbf{C}^\dagger(2\pi\boldsymbol{\kappa})$ , with  $\boldsymbol{\kappa}$  any integer vector.

Equations 37 show that  $\mathbf{C} = [ \mathbf{M} \mid \mathbf{Id} ]$ . The integer vector  $\boldsymbol{\mu} \triangleq \begin{bmatrix} 0 \\ \boldsymbol{\kappa} \end{bmatrix}$  is then such that

$$\mathbf{C}\boldsymbol{\mu} = [ * \mid \mathbf{Id} ] \begin{bmatrix} 0 \\ \boldsymbol{\kappa} \end{bmatrix} = \boldsymbol{\kappa}.$$

Then we have:

$$\begin{aligned}
C\boldsymbol{\mu} = \boldsymbol{\kappa} &\Rightarrow C\boldsymbol{\mu}' = CC^\dagger\boldsymbol{\kappa} \\
&\Rightarrow C(C^\dagger\boldsymbol{\kappa} - \boldsymbol{\mu}) = 0 \\
&\Rightarrow \exists\boldsymbol{\alpha}_2, C^\dagger\boldsymbol{\kappa} - \boldsymbol{\mu} = B\boldsymbol{\alpha}_2 \\
&\Rightarrow \exists\boldsymbol{\alpha}_2, 2\pi C^\dagger\boldsymbol{\kappa} = 2\pi\boldsymbol{\mu} + B(2\pi\boldsymbol{\alpha}_2) \\
&\Rightarrow \exists\boldsymbol{\alpha}_2, C^\dagger(0 [2\pi]) + \bar{B}\boldsymbol{\alpha}_1 \equiv B(\underbrace{2\pi\boldsymbol{\alpha}_2 + \boldsymbol{\alpha}_1}_{\boldsymbol{\alpha}}) [2\pi].
\end{aligned}$$

So equation 46 yields

$$\exists\boldsymbol{\alpha}, \boldsymbol{\phi}^{\text{ker}} \equiv \bar{B}\boldsymbol{\alpha} [2\pi] \quad (47)$$

#### D. Square-root of a Gaussian distribution

Let us suppose we measure the squared value  $s$  of a positive value  $a$ , with an additive Gaussian noise:

$$s^{\text{data}} = a^2 + s^{\text{noise}}, \quad (48)$$

$s^{\text{noise}}$  being 0 mean Gaussian with the variance  $\sigma_s^2$ . Let  $\hat{a}$  be the estimator of  $a$  from  $s^{\text{data}}$  defined by

$$\hat{a} = \begin{cases} \sqrt{s^{\text{data}}}, & \text{if } s^{\text{data}} > 0 \\ 0 & \text{else} \end{cases}$$

$\hat{a}$  can be seen as pseudo-data. The data model of  $\hat{a}$  derived from equation 48 is not additive Gaussian. As will be shown in section E, an optimal Gaussian approximation of the data model of  $\hat{a}$  would be:

$$\hat{a} = a + a^{\text{noise}}, \quad (49)$$

with  $a^{\text{noise}}$  a Gaussian noise with a mean equal to  $\langle \hat{a} \rangle$  and a standard deviation  $\sqrt{\text{Var}(\hat{a})}$ .

We have studied the behavior of the mean  $\langle \hat{a} \rangle$  and standard deviation  $\sqrt{\text{Var}(\hat{a})}$  of this estimator for various values of  $a^2$ , with a unit  $\sigma_s$  (see figs. 7 and 8).

We can distinguish two regimes for  $\langle \hat{a} \rangle$ :

- a low mean regime, where  $a^2 \leq \sigma_s/6$ : a non negligible part of the distribution of  $s^{\text{data}}$  around  $a^2$  is in the negative domain. Because  $\hat{a}$  estimates a null value for  $a$  when  $s^{\text{data}}$  is negative, its mean will mainly depend on the width of the Gaussian wings. A good approximation of  $\langle \hat{a} \rangle$  is  $\sqrt{\sigma_s/6}$ ;
- a high mean regime, where  $a^2 \geq \sigma_s/6$ : the most part of the distribution of  $s^{\text{data}}$  around  $a^2$  is in the positive domain. The fact that  $\hat{a}$  estimates a null value for  $a$  when  $s^{\text{data}} < 0$  does not impact its mean  $\langle \hat{a} \rangle$ , which is close to  $a$ . Because  $a$  is not known, we choose  $\langle \hat{a} \rangle = \sqrt{s^{\text{data}}}$ .

We can distinguish the same two regimes for  $\sqrt{\text{Var}(\hat{a})}$ . However, the transition is around  $\sigma_s$ :

- when  $a^2 \leq \sigma_s$ , the fact that  $\hat{a}$  estimates a null value for  $a$  when  $s^{\text{data}}$  is negative tends to diminish its standard deviation, which we approximate by  $\sqrt{\text{Var}(\hat{a})} \simeq \sqrt{\sigma_s}/2$ ;

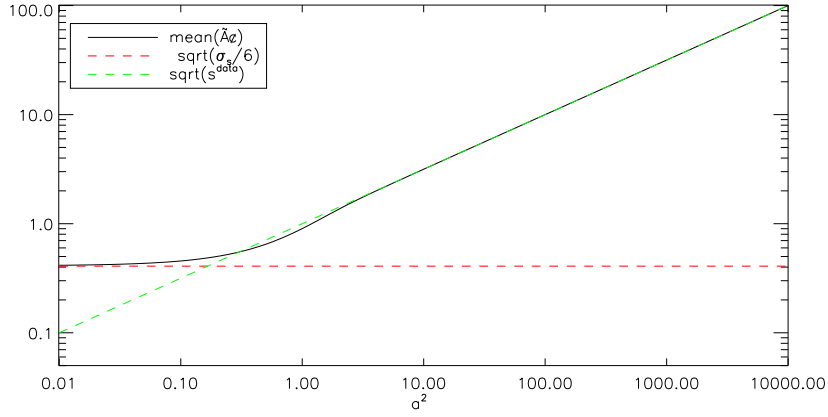


Fig. 7. Behavior of  $\langle \hat{a} \rangle$  in function of  $a^2$  with a unit  $\sigma_s$

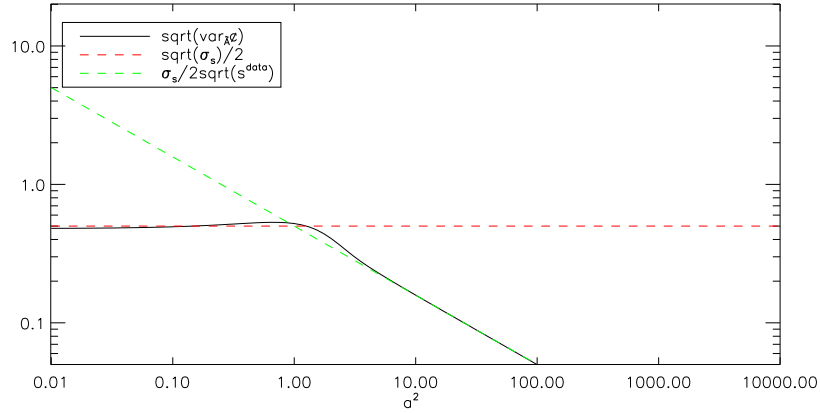


Fig. 8. Behavior of  $\sqrt{\text{Var}(\hat{a})}$  in function of  $a^2$  with a unit  $\sigma_s$

- in the high mean regime, where  $a^2 \geq \sigma_s$ , the most part of the distribution of  $s^{\text{data}}$  around  $a^2$  is in the positive domain, and  $\sqrt{\text{Var}(\hat{a})}$  is close to the classical expression. This expression corresponds to a first order expansion in  $\sigma_a$ :

$$(a + \sigma_a)^2 = a^2 + \sigma_s \Rightarrow 2a\sigma_a \simeq \sigma_s.$$

$\sigma_s/2a$ . Because  $a$  is not known, we choose  $\sqrt{\text{Var}(\hat{a})} = \sigma_s/2\sqrt{s^{\text{data}}}$ .

We then propose the pseudo-data model

$$a^{\text{data}} = a + a^{\text{noise}}$$

with  $a^{\text{data}} = \begin{cases} \sqrt{s^{\text{data}}}, & \text{if } s^{\text{data}} > 0 \\ 0 & \text{else} \end{cases}$  and  $a^{\text{noise}}$  a Gaussian noise with mean and standard devi-

ation defined by with :

$$\bar{a} = \begin{cases} \sqrt{\sigma_s/6}, & \text{if } s^{\text{data}} \leq \sigma_s/6 \\ \sqrt{s^{\text{data}}}, & \text{if } s^{\text{data}} \geq \sigma_s/6 \end{cases}$$

$$\sigma_a = \begin{cases} \sqrt{\sigma_s}/2 & \text{if } s^{\text{data}} \leq \sigma_s \\ \frac{\sigma_s}{2\sqrt{s^{\text{data}}}}, & \text{if } s^{\text{data}} \geq \sigma_s \end{cases}$$

We also decide to discard the data such that  $s^{\text{data}} \leq -\sigma_s$ .

## E. Cartesian Gaussian approximation to a polar Gaussian distribution

If we define

$$\mathbf{y}_{\alpha(t)}(\mathbf{x}, t) \triangleq \mathbf{H}(t)\mathbf{x} \cdot e^{i\bar{B}\alpha(t)}, \quad (50)$$

equation (31) reads

$$\begin{cases} \mathbf{a}^{\text{data}}(t) = |\mathbf{y}_{\alpha(t)}|(\mathbf{x}, t) + \mathbf{a}^{\text{noise}}(t), & \mathbf{a}^{\text{noise}}(t) \sim \mathcal{N}(\mathbf{0}, \mathbf{R}_{\mathbf{a}(t)}) \\ \phi^{\text{data}}(t) \stackrel{2\pi}{\equiv} \arg \mathbf{y}_{\alpha(t)}(\mathbf{x}, t) + \phi^{\text{noise}}(t), & \phi^{\text{noise}}(t) \sim \mathcal{N}(\mathbf{0}, \mathbf{R}_{\phi(t)}) \end{cases} \quad (51)$$

### E.A. General expression

With consider a polar distribution of a Gaussian vector  $\mathbf{y}$  of modulus  $\mathbf{a}$  and phase  $\phi$ :

$$\phi^{\text{data}} = \bar{\phi} + \phi^{\text{noise}} \quad (52)$$

$$\mathbf{a}^{\text{data}} = \bar{\mathbf{a}} + \mathbf{a}^{\text{noise}} \quad (53)$$

where  $\phi^{\text{noise}}$  and  $\mathbf{a}^{\text{noise}}$  are 0 mean real Gaussian vectors, of covariance matrices  $\mathbf{R}_{\mathbf{a}}$  and  $\mathbf{R}_{\phi}$  (the vectors  $\phi^{\text{noise}}$  and  $\mathbf{a}^{\text{noise}}$  are supposed uncorrelated).

With the definitions

$$\left\{ \begin{array}{l} \bar{\mathbf{y}} \triangleq \bar{\mathbf{a}} \exp i\bar{\phi} \\ \mathbf{y}^{\text{noise}} \triangleq \mathbf{y}^{\text{data}} - \bar{\mathbf{y}} \\ \mathbf{y}_{\text{rad}}^{\text{n}} \triangleq \Re \left\{ \mathbf{y}^{\text{noise}} e^{-i\bar{\phi}} \right\} \\ \mathbf{y}_{\text{tan}}^{\text{n}} \triangleq \Im \left\{ \mathbf{y}^{\text{noise}} e^{-i\bar{\phi}} \right\} \\ \bar{\mathbf{y}}^{\text{noise}} \triangleq \begin{bmatrix} \mathbf{y}_{\text{rad}}^{\text{n}} \\ \mathbf{y}_{\text{tan}}^{\text{n}} \end{bmatrix} \end{array} \right. \quad (54)$$

we gather:

$$\begin{cases} \mathbf{y}_{\text{rad}}^{\text{n}} = [\bar{\mathbf{a}} + \mathbf{a}^{\text{noise}}] \cos \phi^{\text{noise}} - \bar{\mathbf{a}} \\ \mathbf{y}_{\text{tan}}^{\text{n}} = [\bar{\mathbf{a}} + \mathbf{a}^{\text{noise}}] \sin \phi^{\text{noise}} \end{cases} \quad (55)$$

A complex vector is Gaussian if and only if each of its components is Gaussian. A complex is Gaussian if and only if, in any Cartesian basis, its two components are Gaussian. So  $\mathbf{y}$  is Gaussian if and only if  $\bar{\mathbf{y}}^{\text{noise}}$  is Gaussian, which is not the case[20]. In what follows, we show how to optimally approximate the distribution of  $\bar{\mathbf{y}}^{\text{noise}}$  by a Gaussian distribution.

### E.B. Gaussian Approximation

We characterize our Cartesian additive Gaussian approximation, *i.e.* its mean  $\langle \bar{\mathbf{y}}^{\text{noise}} \rangle$  and covariance  $\mathbf{R}_{\bar{\mathbf{y}}^{\text{noise}}}$ , by minimizing the Kullback-Leibler distance between the two noise distributions, which gives [20]:

$$\begin{cases} \langle \bar{\mathbf{y}}^{\text{noise}} \rangle = E \left\{ \begin{bmatrix} \mathbf{y}_{\text{rad}}^{\text{n}} \\ \mathbf{y}_{\text{tan}}^{\text{n}} \end{bmatrix} \right\} = \begin{bmatrix} \bar{\mathbf{y}}_{\text{rad}}^{\text{n}} \\ \bar{\mathbf{y}}_{\text{tan}}^{\text{n}} \end{bmatrix} \\ \mathbf{R}_{\bar{\mathbf{y}}^{\text{noise}}} = E \left\{ \begin{bmatrix} \bar{\mathbf{y}}_{\text{rad}}^{\text{n}} - \mathbf{y}_{\text{rad}}^{\text{n}} \\ \bar{\mathbf{y}}_{\text{tan}}^{\text{n}} - \mathbf{y}_{\text{tan}}^{\text{n}} \end{bmatrix} \begin{bmatrix} \bar{\mathbf{y}}_{\text{rad}}^{\text{n}} - \mathbf{y}_{\text{rad}}^{\text{n}} \\ \bar{\mathbf{y}}_{\text{tan}}^{\text{n}} - \mathbf{y}_{\text{tan}}^{\text{n}} \end{bmatrix}^{\text{T}} \right\} \end{cases} \quad (56)$$

and we define

$$\mathbf{R}_{\bar{\mathbf{y}}^{\text{noise}}} \triangleq \begin{bmatrix} \mathbf{R}_{\text{rad,rad}} & \mathbf{R}_{\text{rad,tan}} \\ \mathbf{R}_{\text{rad,tan}}^{\text{T}} & \mathbf{R}_{\text{tan,tan}} \end{bmatrix}$$

For a 0 mean Gaussian vector  $\phi^{\text{noise}}$  of covariance matrix  $\mathbf{R}_{\phi}$ ,

$$\begin{aligned} E \{ \sin \phi_i^{\text{noise}} \} &= 0 \\ E \{ \cos \phi_i^{\text{noise}} \} &= \exp -\frac{\mathbf{R}_{\phi_{ii}}}{2} \\ E \{ \sin \phi_i^{\text{noise}} \sin \phi_j^{\text{noise}} \} &= \sinh \mathbf{R}_{\phi_{ij}} \cdot \exp -\frac{\mathbf{R}_{\phi_{ii}} + \mathbf{R}_{\phi_{jj}}}{2} \\ E \{ \cos \phi_i^{\text{noise}} \cos \phi_j^{\text{noise}} \} &= \cosh \mathbf{R}_{\phi_{ij}} \cdot \exp -\frac{\mathbf{R}_{\phi_{ii}} + \mathbf{R}_{\phi_{jj}}}{2} \\ E \{ \cos \phi_i^{\text{noise}} \sin \phi_j^{\text{noise}} \} &= 0 \end{aligned} \quad (57)$$

By combining equations. 56, 54, 55 and 57, we obtain:

$$\begin{aligned} E \{ \mathbf{y}_{\text{rad}i}^{\text{n}} \} &= \bar{a}_i \left[ e^{-\frac{\mathbf{R}_{\phi_{ii}}}{2}} - 1 \right] \\ E \{ \mathbf{y}_{\text{tan}i}^{\text{n}} \} &= 0 \\ [\mathbf{R}_{\text{rad,rad}}]_{ij} &= \left[ \bar{a}_i \bar{a}_j \left( \cosh \mathbf{R}_{\phi_{ij}} - 1 \right) + \mathbf{R}_{a_{ij}} \cosh \mathbf{R}_{\phi_{ij}} \right] \cdot e^{-\frac{\mathbf{R}_{\phi_{ii}} + \mathbf{R}_{\phi_{jj}}}{2}} \\ [\mathbf{R}_{\text{rad,tan}}]_{ij} &= 0 \\ [\mathbf{R}_{\text{tan,tan}}]_{ij} &= \left( \bar{a}_i \bar{a}_j + \mathbf{R}_{a_{ij}} \right) \sinh \mathbf{R}_{\phi_{ij}} \cdot e^{-\frac{\mathbf{R}_{\phi_{ii}} + \mathbf{R}_{\phi_{jj}}}{2}} \end{aligned} \quad (58)$$

### E.C. The scalar case

Now, we make the additional assumption that both  $\phi^{\text{noise}}$  and  $\mathbf{a}^{\text{noise}}$  are decorrelated, *i.e.*

$$\begin{cases} \mathbf{R}_{\mathbf{a}} = \text{Diag} \{ \sigma_{a,i}^2 \} \\ \mathbf{R}_{\phi} = \text{Diag} \{ \sigma_{\phi,i}^2 \} \end{cases}$$

We obtain:

$$\begin{cases} \mathbf{R}_{\text{rad,rad}} = \text{Diag} \{ \sigma_{\text{rad},i}^2 \} \\ \mathbf{R}_{\text{tan,tan}} = \text{Diag} \{ \sigma_{\text{tan},i}^2 \} \\ \mathbf{R}_{\text{rad,tan}} = 0 \end{cases}$$

with

$$\begin{aligned} \sigma_{\text{rad},i}^2 &= \frac{\bar{a}_i^2}{2} \left( 1 - e^{-\sigma_{\phi,i}^2} \right)^2 + \frac{\sigma_{a,i}^2}{2} \left( 1 + e^{-2\sigma_{\phi,i}^2} \right) \\ \sigma_{\text{tan},i}^2 &= \frac{\bar{a}_i^2}{2} \left( 1 - e^{-2\sigma_{\phi,i}^2} \right) + \frac{\sigma_{a,i}^2}{2} \left( 1 - e^{-2\sigma_{\phi,i}^2} \right) \end{aligned} \quad (59)$$

In this case, we can plot for one complex visibility the true noise distribution - i.e. a Gaussian noise in phase and modulus - and our Gaussian approximation (see fig. 1).

## F. Acknowledgments

The authors want to express their special thanks to Eric Thiébaud for his support and for letting them use his minimization software. Serge Meimon is very grateful to Guy Perrin and Sylvestre Lacour, who allowed him to participate to two IOTA observing campaigns. We also would like to thank all the people who contributed to the existence and success of the IOTA interferometer, in particular John Monnier, Wes Traub, Jean-Philippe Berger and Marc Lacasse. Serge Meimon also thanks Vincent Bix Josso for his help on appendix B. Serge Meimon and Laurent Mugnier acknowledge support from PHASE, the space and ground based high angular resolution partnership between ONERA, Observatoire de Paris, CNRS and University Denis Diderot Paris 7.

Corresponding author Serge Meimon can be reached at [Serge.Meimon@onera.fr](mailto:Serge.Meimon@onera.fr)

## References

1. J. D. Monnier, “An Introduction to Closure Phases,” in *Principles of Long Baseline Stellar Interferometry*, P. R. Lawson, ed., chap. 13, pp. 203–239 (Jet Propulsion Laboratory, 1999).
2. Thompson, Moran, and Swenson, *Interferometry and synthesis in Radio-astronomy* (Wiley Interscience, New-York, 1986).
3. A. Lannes, E. Anterrieu, and P. Maréchal, “Clean and Wipe,” *Astron. Astrophys. Suppl. Ser.* **123**, 183–198 (1997).
4. J. Hogbom, “Aperture synthesis with a non-regular distribution of interferometer baselines,” *Astron. Astrophys. Suppl. Ser.* **15**, 417–426 (1974).
5. T. J. Cornwell and P. N. Wilkinson, “A new method for making maps with unstable radio interferometers,” *Mon. Not. R. Astr. Soc.* **196**, 1067–1086 (1981).
6. A. Lannes, “Weak-phase imaging in optical interferometry,” *J. Opt. Soc. Am. A* **15**(4), 811–824 (1998).
7. J. W. Goodman, *Statistical Optics* (Wiley-Interscience, 1985).
8. D. L. Fried, “Statistics of a Geometric Representation of Wavefront Distortion,” *J. Opt. Soc. Am.* **55**(11), 1427–1435 (1965).
9. A. Quirrenbach, “Phase Referencing,” in *Principles of Long Baseline Stellar Interferometry*, P. R. Lawson, ed., chap. 9, pp. 143–160 (Jet Propulsion Laboratory, 1999).

10. R. C. Jennison, "A phase sensitive interferometer technique for the measurement of the Fourier transforms of spatial brightness distribution of small angular extent," *Mon. Not. R. Astr. Soc.* **118**, 276–284 (1958).
11. T. A. Pauls, J. S. Young, W. D. Cotton, and J. D. Monnier, "A Data Exchange Standard for Optical (Visible/IR) Interferometry," *Publications of the Astronomical Society of the Pacific* **117**(837), 1255–1262 (2005).
12. G. Perrin, "The calibration of interferometric visibilities obtained with single-mode optical interferometers. Computation of error bars and correlations," *Astron. Astrophys.* **400**, 1173–1181 (2003).
13. C. Haniff, "Least-squares Fourier phase estimation from the modulo  $2\pi$  bispectrum phase," *JOSA* **8**(1), 134–140 (1991).
14. G. Le Besnerais, S. Lacour, L. M. Mugnier, E. Thiébaud, G. Perrin, and S. Meimon, "Advanced Imaging Methods for Long-Baseline Optical Interferometry," *IEEE Journal of Selected Topics in Signal Processing* **2** (2008).
15. G. Demoment, "Image Reconstruction and Restoration: Overview of Common Estimation Structures and Problems," *IEEE Trans. Acoust. Speech Signal Process.* **37**(12), 2024–2036 (1989).
16. R. Nityananda and R. Narayan, "Maximum Entropy Image Reconstruction-A practical Non-Information-Theoretic Approach," *J. Astrophys. Astr.* **3**, 419–450 (1982).
17. E. Thiébaud, P. J. V. Garcia, and R. Foy, "Imaging with Amber/VLTI: the case of microjets," *Astrophys. Space. Sci.* **286**, 171–176 (2003).
18. J. Navaza, "Accurate solutions of the maximum entropy equations. Their impact on the foundations of direct methods." pp. 317–323 (1991).
19. Y. Bar-Shalom and X.-R. Li, *Multitarget-multisensor tracking: Principles and techniques* (YBS Publishing, Storrs, CT., 1995).
20. S. Meimon, L. M. Mugnier, and G. Le Besnerais, "A convex approximation of the likelihood in optical interferometry," *J. Opt. Soc. Am. A* (2005).
21. L. M. Mugnier, G. Le Besnerais, and S. Meimon, "Inversion in Optical Imaging through Atmospheric Turbulence," in *Bayesian Approach to Inverse Problems*, J. Idier, ed., Digital Signal and Image Processing Series, chap. 10, pp. 243–283 (ISTE / John Wiley, London, 2008).
22. A. Lannes, "Integer ambiguity resolution in phase closure imaging," *Optical Society of America Journal A* **18**, 1046–1055 (2001).
23. P. R. Lawson, W. D. Cotton, C. A. Hummel, J. D. Monnier, M. Zhao, J. S. Young, H. Thorsteinsson, S. C. Meimon, L. Mugnier, G. Le Besnerais, E. Thiébaud, and P. G. Tuthill, "An interferometry imaging beauty contest," vol. 5491, pp. 886–899 (SPIE, 2004).
24. J. A. Benson, C. A. Hummel, and D. Mozurkewich, "Simultaneous 6-station observations with the NPOI," vol. 4838, pp. 358–368 (SPIE, 2003).
25. F. P. Schloerb, J.-P. Berger, N. P. Carleton, P. Hagenauer, P. Y. Kern, P. R. Labeye, M. G. Lacasse, F. Malbet, R. Millan-Gabet, J. D. Monnier, M. R. Pearlman, E. Pedretti, K. Rousset-Perraut, S. D. Ragland, P. A. Schuller, W. A. Traub, and G. Wallace, "IOTA: recent science and technology," vol. 6268, p. 62680I (SPIE, 2006).
26. G. Perrin, S. Ridgway, B. Mennesson, W. Cotton, J. Woillez, T. Verhoelst, P. Schuller, V. Coudé du Foresto, W. Traub, R. Millan-Galbet, and M. Lacasse, "Unveiling Mira stars behind the molecules. Confirmation of the molecular layer model with narrow band near-infrared



interferometry,” *Astron. Astrophys.* **426**, 279–296 (2004).

27. S. Lacour, “Imagerie des étoiles évoluées par interférométrie. Réarrangement de pupille,” Ph.D. thesis, Univ. Paris VI (2007).

## List of Figures

1	Contour plots of a polar Gaussian distribution and of its Cartesian Gaussian approximation . . . . .	11
2	WISARD algorithm loop . . . . .	12
3	Synthetic object (right) and frequency coverage (left) from the Imaging Beauty Contest 2004 . . . . .	14
4	Reconstructions with WISARD. Upper row : under-regularized quadratic model (left), over-regularized quadratic model (center), quadratic model with correct regularization parameter (right). Lower row : white $L_2L_1^w$ model with automatically set scale and delta parameters (left), white $L_2L_1^w$ model with half scale (center), white $L_2L_1^w$ model with half delta (right). Each image field is $12.1 \times 12.1$ mas. . . . .	15
5	Goodness of fit at WISARD convergence. . . . .	16
6	Frequency coverage (left) and reconstruction of the star $\chi$ Cygni (right). . . . .	16
7	Behavior of $\langle \hat{a} \rangle$ in function of $a^2$ with a unit $\sigma_s$ . . . . .	20
8	Behavior of $\sqrt{\text{Var}(\hat{a})}$ in function of $a^2$ with a unit $\sigma_s$ . . . . .	20